VNU Journal of Science: Mathematics - Physics
Journal homepage: https://js.vnu.edu.vn/MaP

Original Article

Enhanced A549 and HeLa Cell Separation Using a Ferromagnetic Strip-integrated Microfluidic Magnetophoresis System

Nguyen Van Phu[1], Bui Van Anh[1], Phan Hoang Anh[2], Tran Thanh Hang[2], Pham Van Thanh[1], Chun-Ping Jen[3,4], Bui Thanh Tung[2], Do Quang Loc[2], Chu Duc Trinh[2,*]

[1]VNU University of Science, 334 Nguyen Trai, Thanh Xuan, Hanoi, Vietnam
[2]VNU University of Engineering and Technology, 144 Xuan Thuy, Cau Giay, Hanoi, Vietnam
[3]Department of Mechanical Engineering and Advanced Institute of Manufacturing for High-Tech Innovations, National Chung Cheng University, 168 University Road, Min-Hsiung Township, Chiayi 621301, Taiwan, ROC
[4]School of Dentistry, College of Dental Medicine, Kaohsiung Medical University, 100 Shih-Chuan 1st Road, Sanmin District, Kaohsiung 80708, Taiwan, ROC

Received 10th March 2025
Revised 05th June 2025; Accepted 25th July 2025

Abstract: In this work, a microfluidic platform integrating magnetophoresis for the separation of A549 lung cancer cells from HeLa cervical cancer cells was developed. The platform was utilized with the lateral magnetophoresis, leveraging ferromagnetic strips embedded in the microchannel to generate magnetic gradients. A549 cells, labeled with magnetic beads (MBs), were selectively deflected under magnetic force, while unlabeled HeLa cells followed the default hydrodynamic path. The separation chamber was designed to direct magnetic-labeled cells to the target outlet and unlabeled cells to the non-target outlet. Experimental results showed that the efficiency of A549 cell separation increased progressively over time, reaching up to 84.4% with minimal contamination from HeLa cells. This enhancement is attributed to the gradual stabilization of flow and internal conditions within the microchannel, enabling more consistent cell deflection and collection. These findings demonstrate the platform's capability for high-purity cell sorting and highlight its strong potential for integration into lab-on-a-chip systems for cancer diagnostics and therapeutic monitoring at the point of care.

Keywords: Microfluidic platform, Magnetophoresis, Cell separation, Magnetic nanobeads (MNBs), cancer diagnostics.

* Corresponding author.
E-mail address: trinhcd@vnu.edu.vn

https//doi.org/10.25073/2588-1124/vnumap.4994

1. Introduction

Lung cancer is one of the most common and deadly cancers worldwide, responsible for approximately 1.8 million deaths each year [1]. Early detection plays a critical role in improving the prognosis and survival rates of lung cancer patients [2, 3]. While conventional diagnostic methods such as tissue biopsies and imaging techniques remain important, they are often invasive and may not provide sufficient sensitivity for early-stage detection [4]. Liquid biopsy, a less invasive alternative, has gained significant interest due to its ability to detect cancer-specific biomarkers in blood samples, providing crucial insights into disease progression and treatment responses [5, 6]. Among the various biomarkers, circulating tumor cells (CTCs) are considered a promising target for the early detection and monitoring of cancers, including lung cancer [7, 8].

CTCs are cancerous cells that have detached from primary or metastatic tumors and entered the bloodstream. Due to their extremely low concentration, approximately one CTC per billion normal blood cells, the efficient isolation of these cells remains technically challenging [9, 10]. Several conventional techniques have been explored for separating CTCs, including size-based filtration, density gradient centrifugation, and fluorescence-activated cell sorting (FACS) [11, 12]. However, these methods often exhibit limitations such as low purity, reduced viability of recovered cells, and complex sample preparation procedures [13, 14]. To address these issues, label-based separation methods, particularly magnetophoresis, have attracted considerable interest. Magnetophoresis employs magnetic beads (MBs) to selectively label specific target cells, facilitating their separation under an applied magnetic field. This approach provides distinct advantages over traditional methods, including higher specificity, minimal impact on cell viability, and suitability for integration into microfluidic platforms [15, 16]. Lateral magnetophoresis, which utilizes lateral magnetic forces to guide MP-labeled CTCs away from unlabeled cells, has demonstrated significant promise in terms of accuracy and ease of integration into lab-on-a-chip (LOC) devices [17, 18]. LOC systems are particularly appealing in biomedical research due to their capability to manage small fluid volumes, thereby enabling rapid and efficient cell separation while minimizing reagent usage [19].

In recent years, microfluidic devices integrating magnetophoresis with LOC technology have demonstrated superior performance in isolating rare cells, such as CTCs, from complex biological fluids. These platforms offer highly controlled microenvironments that enable precise tuning of magnetic fields to achieve efficient, high-purity cell separation [12]. Specifically, lateral magnetophoresis systems, incorporating ferromagnetic elements within microchannels, effectively direct magnetically labeled CTCs into designated collection outlets while minimizing contamination from non-labeled cells [17, 18]. Despite these advances, current magnetophoretic separation methods still face limitations. One major challenge is the extremely low abundance of CTCs in peripheral blood, often ranging from 1 to 100 CTCs per milliliter, which complicates their detection and isolation [20]. Additionally, the heterogeneity of CTCs, including variations in size, deformability, and surface marker expression, can lead to inconsistent capture efficiencies [21]. For instance, CTCs undergoing epithelial-to-mesenchymal transition (EMT) may downregulate epithelial markers like EpCAM, reducing the efficacy of antibody-based magnetic labeling strategies [22]. Addressing these limitations is crucial for expanding the applicability of microfluidic magnetophoresis platforms in clinical settings. Future research should focus on developing more robust and versatile systems capable of handling the heterogeneity of CTC populations, minimizing non-specific interactions, and ensuring high viability of isolated cells.

In this work, a novel microfluidic platform integrating lateral magnetophoresis was developed for the efficient separation of A549 lung cancer cells from HeLa cervical cancer cells. The platform features embedded ferromagnetic strips within microchannels, generating controlled magnetic field gradients that selectively guide magnetically labeled A549 cells towards a distinct collection outlet. Concurrently, unlabeled HeLa cells remain unaffected, following the primary flow trajectory. Systematic optimization

of magnetic field intensity and fluid flow dynamics significantly enhanced the efficiency and purity of cell isolation, achieving minimal cross-contamination. The developed approach is minimally invasive, rapid, and demonstrates superior selectivity, underscoring its potential for clinical cancer diagnostics and therapeutic applications. By integrating advanced microfluidic manipulation with magnetic cell separation techniques, the system supports real-time monitoring of disease progression and contributes to precision medicine approaches. Moreover, its compatibility with LOC technologies further highlights the platform's suitability for translation into clinical settings, notably in facilitating early-stage cancer detection and enabling tailored therapeutic interventions.

2. Materials and Method

2.1. Materials

Magnetic beads were employed for immobilization on the surface of A549 lung cancer cells through an aptamer-magnetic bead complex. Initially, magnetic beads were washed three times with phosphate-buffered saline (PBS, 10X) provided by Thermo Fisher Scientific, ensuring the removal of any impurities. Subsequently, the bead surfaces were functionalized using a mixture of PBS and EDC (1-Ethyl-3-(3-dimethylaminopropyl)carbodiimide)/NHS (N-Hydroxysuccinimide) sourced from Sigma-Aldrich. Simultaneously, an NH_2-aptamer sequence 5'-ACGC TCGG ATGC CACT ACAG GGTT GCAT GCCG TGGG GAGG GGGG TGGG TTTT ATAG CGTA CTCA GCTC ATGG ACGT GCTG GTGA C-3', modified with a 5'-NH_2 group was prepared by centrifugation and mixed with a binding buffer containing bovine serum albumin (BSA), $MgCl_2$, and yeast tRNA, all diluted in 1X PBS prepared using ultrapure water from a Milli-Q Direct-Q system provided by Millipore Simplicity. A549 cells were cultured in Dulbecco's Modified Eagle Medium (DMEM) containing $NaHCO_3$ and fetal bovine serum (FBS), all sourced from Sigma-Aldrich, which facilitated the immobilization of magnetic beads onto the cells. Additionally, the electroplating setup included a comprehensive range of chemicals and equipment for nickel-iron coating. The electroplating solution was prepared, incorporating Nickel (II) sulfate hexahydrate, Iron (II) sulfate heptahydrate and related substance provided by Merck Millipore, Thermo Fisher Scientific. Boric acid was used as a buffering agent, while Ammonium chloride and Sodium benzenesulfonate were added to enhance conductivity and reduce surface tension, respectively, aiding in a more uniform metal deposition. Sodium chloride was also included to increase the ionic strength of the solution, crucial for facilitating the electroplating kinetics. This detailed and controlled preparation was pivotal in achieving a uniform and efficient deposition process.

2.2. Device Design and Fabrication

The microfluidic chip employed in this work was designed to include a separation chamber and flow channels, fabricated on a polydimethylsiloxane (PDMS) substrate adhered to a glass slide, as shown in Fig. 1. A key component of this chip is the lateral magnetophoretic microseparator, which consists of a bottom glass substrate embedded with a ferromagnetic permalloy wire array. The wire array is positioned at an angle of 6° relative to the flow direction to optimize the magnetic separation. When an external magnetic field is applied uniformly, a high-gradient magnetic field is generated at the edges of the wire, enhancing the precision of the separation process. The channel widths of the microfluidic chip were carefully designed to maximize target cell purity and optimize flow rates into the impedance cytometer. Outlet 1 is a narrow channel with a width of 200 µm, and it removes non-target constituents such as normal blood cells and other unlabeled debris. Outlet 2 is wider at 800 µm, and it selectively captures circulating tumor cells that have been labeled with magnetic beads. As the target CTCs flow

through the microchannel, they experience both magnetic (F_m) and hydrodynamic (F_d) forces. These forces combine to produce a lateral magnetic force (F_l), which directs the target CTCs toward outlet 2, while non-target components are directed toward outlet 1.

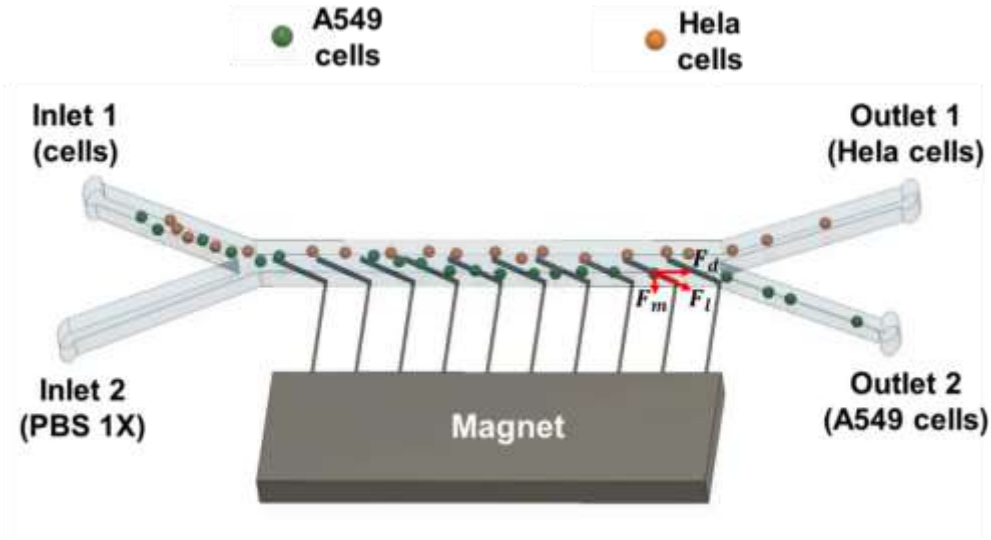

Figure 1. 3D image of the proposed structure.

The fabrication of both the gold electrodes and the microchannels used in the microfluidic system involves a series of precise steps to ensure the device's functionality, with the detailed process illustrated in Fig.2. The process begins with the gold electrode fabrication, which utilizes a wet etching method. A glass substrate is prepared by sequentially evaporating chromium and gold layers with respective thicknesses of 20 nm and 100 nm. The chromium layer acts as an adhesive for the gold on the glass surface. A layer of S1813 photoresist is then spin-coated onto the substrate at 700 rpm for 10 seconds, followed by 1700 rpm for 20 seconds, resulting in a 2 µm thick resist. The substrate is baked at 90 °C for 2 minutes, followed by UV exposure at an energy of 90 mJ/cm² and another baking at 90 °C for 3 minutes. The photoresist is developed in a mixture of MP 351 and deionized water (2:9 ratio) for 9 seconds, rinsed with DI water, and dried with nitrogen gas. After heating the substrate at 120 °C for 3 minutes, the unprotected gold is etched with a gold etchant for 15 seconds, and the chromium is etched with a chromium etchant for 10 seconds. Finally, the remaining photoresist is removed using acetone and ethanol, followed by DI water rinsing and nitrogen drying.

After successfully fabricating the gold electrode, the next step involves electroplating with a specific ferromagnetic permalloy mixture, as illustrated in step 7 in Figs. 2 and 3. The process commences with the preparation of a $Ni_{0.8}Fe_{0.2}$ solution, which includes 0.2 M Nickel (II) sulfate hexahydrate ($NiSO_4 \cdot 6H_2O$) and 25 mM Iron (II) sulfate heptahydrate ($FeSO_4 \cdot 7H_2O$) as the primary constituents for the desired alloy composition. Additional components such as 0.4 M Boric acid (H_3BO_3), 0.28 M Ammonium chloride (NH_4Cl), 5.46 M Sodium benzenesulfonate ($C_7H_5NO_3S$), and 51.3 mM Sodium chloride (NaCl) are included to stabilize and optimize the plating bath's chemical properties. These chemicals are dissolved in 300 mL of deionized water to form the electroplating solution.

In the electroplating setup, a power supply is connected to deliver a consistent 2 V for 150 seconds across the gold electrode, which acts as the cathode. The application of voltage to this solution triggers the deposition of the NiFe alloy onto the gold electrode, effectively coating it with a ferromagnetic layer. This electrochemical process creates a dense, uniform layer of permalloy, significantly enhancing the

magnetic properties of the electrode, which is critical for its performance in magnetophoretic applications. The successful deposition is evidenced by the visible change in the electrode's appearance before and after the process, as the ferromagnetic wire becomes embedded within the electrode structure.

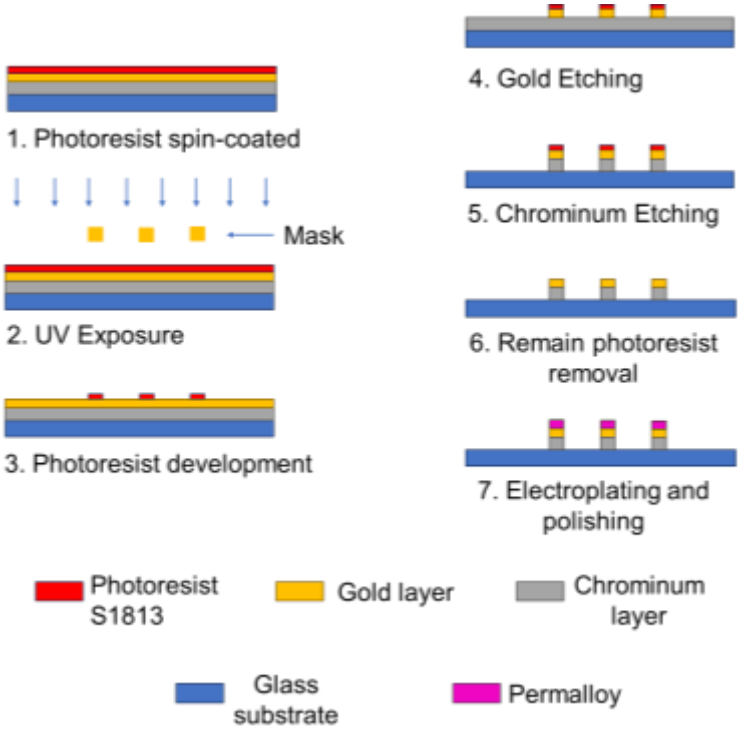

Figure 2. Gold electrode manufacturing process.

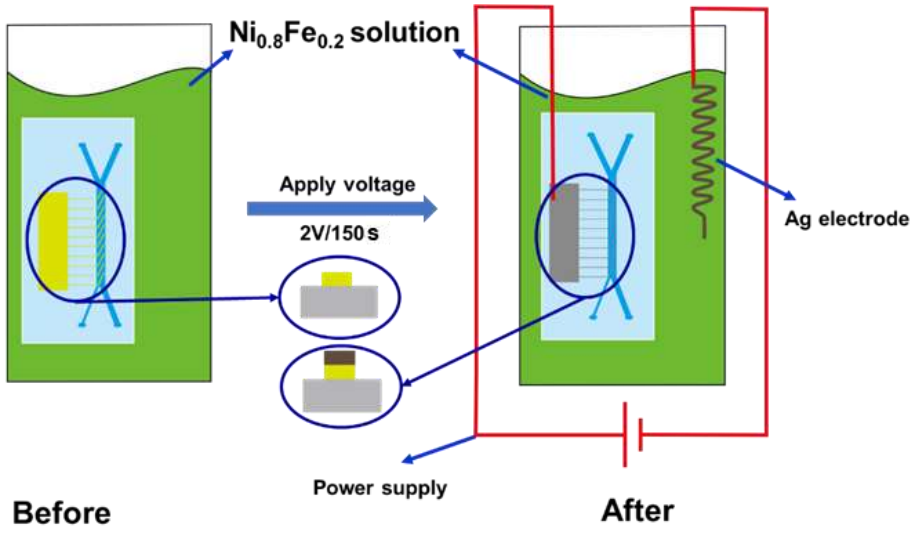

Figure 3. Ferromagnetic permalloy fabrication process.

Finally, the creation of the microchannels utilizes a detailed photolithography technique to construct a mold for casting PDMS. The process starts with applying SU-8 photoresist to a silicon wafer, spinning initially at 500 rpm for 20 seconds, then accelerating to 1000 rpm for 35 seconds to achieve a mold thickness of 100 µm. Following the coating, the wafer is gently heated to 95 °C and maintained for 30 minutes for soft-baking, then allowed to cool to room temperature. UV light exposure through a patterned mask at 200 mJ/cm² is followed by a second baking at the same temperature profile to solidify the pattern. The undeveloped photoresist is then washed away using an SU-8 developer, which exposes the underlying mold. Subsequently, PDMS is prepared in a 10:1 ratio, degassed, and poured onto the fabricated mold. Once cured at 65 °C for two hours, the PDMS is removed to reveal the structured microchannels. Manual creation of inlet and outlet holes is done before the PDMS structure is bonded to a gold electrode-coated glass substrate, enhanced by oxygen plasma treatment to ensure strong adhesion between the surfaces.

2.3. Sample Preparation

In the preparation of samples for this work, magnetic beads were functionalized with a solution comprising PBS, EDC (1-Ethyl-3-(3-dimethylaminopropyl)carbodiimide), and NHS (N-Hydroxysuccinimide), followed by vortex agitation for 15 minutes to achieve a uniform coating. Concurrently, an NH_2-modified aptamer underwent preparation involving centrifugation, heating, and subsequent cooling, after which it was mixed with a binding buffer containing bovine serum albumin (BSA), $MgCl_2$, and yeast tRNA in 1X PBS. This aptamer solution was then combined with the coated magnetic beads and further agitated to promote binding. Separately, A549 lung cancer cells were cultured and subsequently incubated with these aptamer-coated beads. Post-incubation, cells were stained with a green fluorescent dye to enable visualization of bead-cell interactions.

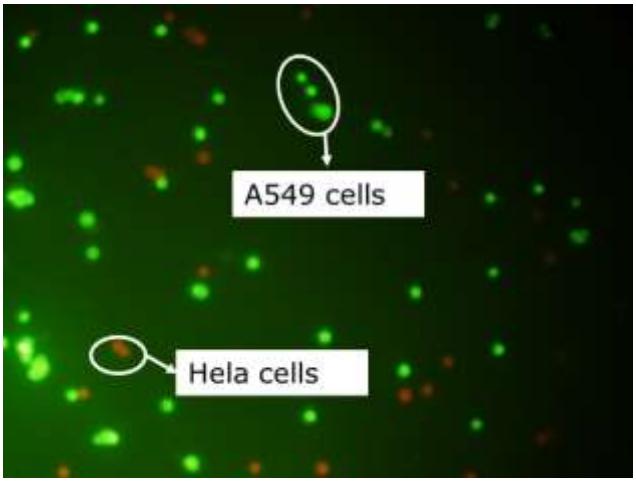

Figure 4. Fluorescent staining of A549 and Hela cells for cell separation analysis.

Fig. 4 illustrates the resulting fluorescently labeled sample, clearly distinguishing two cell populations: A549 cells exhibiting strong green fluorescence and HeLa cells displaying dispersed orange fluorescence. This distinct color differentiation effectively demonstrates successful cell separation, facilitating accurate identification and analysis of each cell type. The described fluorescent staining approach thus provides critical insight into the efficiency of the magnetic bead-cell immobilization and separation processes employed in this research.

3. Results and Discussion

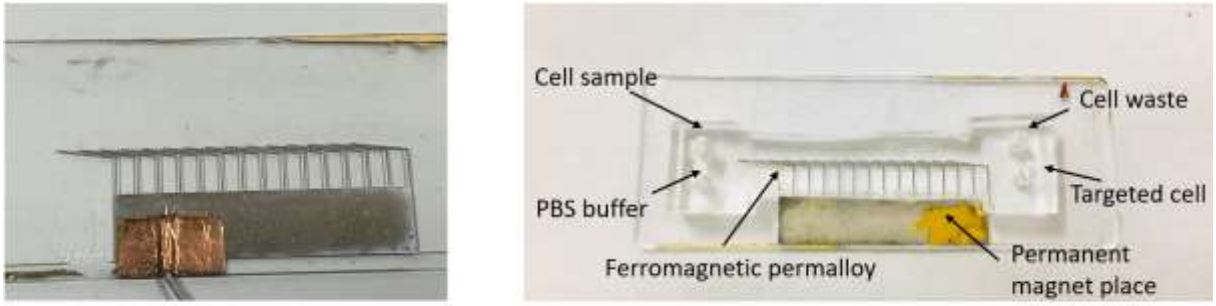

Figure 5. (a) Ferromagnetic permalloy wires, (b) Microfluidic chip on ferromagnetic permalloy.

The successful fabrication of the microfluidic chip, as illustrated by the experimental outcomes, signifies a notable advancement in microscale technologies. Initially, the chip undergoes a critical electroplating process involving a ferromagnetic permalloy, as depicted in Fig. 5(a). This procedure imparts essential magnetic characteristics to the chip, enabling precise control and manipulation of magnetic fields at the microscale. Subsequently, Fig. 5(b) demonstrates the integration of microfluidic channels, which are treated with oxygen plasma to achieve strong adhesion and optimal functionality. This plasma treatment significantly enhances the performance of the chip, enabling efficient handling and processing of cell samples within the microchannel network. Specifically designed to utilize the magnetic properties of the embedded permalloy, these channels facilitate the targeted sorting and separation of cellular components from non-target materials, ensuring precise and efficient cell separation.

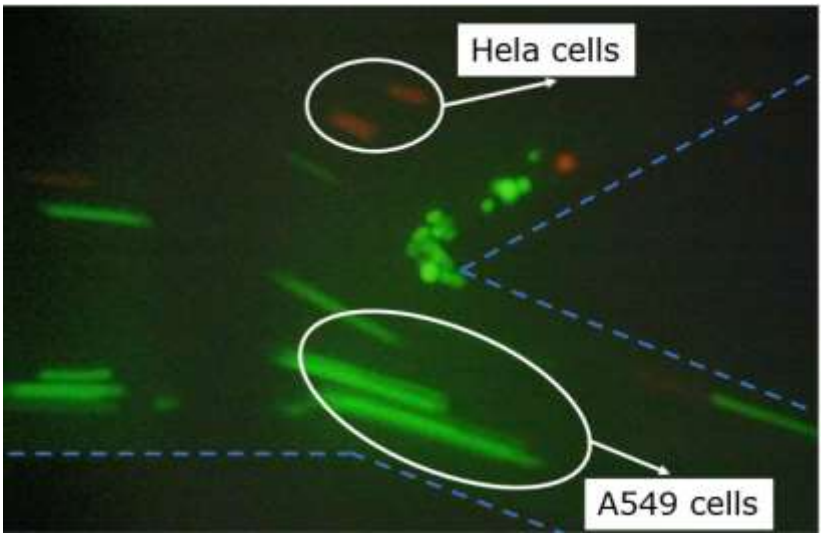

Figure 6. Successful separation of HeLa and A549 cells. This fluorescence microscopy image uses a microfluidic device to effectively isolate HeLa cells (red) and A549 cells (green) post-separation.

Prepared samples containing A549 (target) and HeLa (non-target) cells were introduced into the microfluidic device at a precisely controlled flow rate of 1 µL/min. Upon entering the separation region, cells labeled with MBs, specifically A549 cells, experienced a lateral magnetic force generated by

embedded ferromagnetic strips. This force effectively directed the labeled A549 cells toward a dedicated collection outlet. In contrast, unlabeled HeLa cells, unaffected by the magnetic field, continued along the primary channel path and were subsequently collected at a separate outlet. To further enhance the efficiency of the targeted cell separation, both the flow rate and magnetic field intensity were systematically optimized. Consequently, isolated A549 cells were effectively collected at their designated outlet and promptly prepared for subsequent analytical or culturing procedures. The microfluidic chip demonstrated significant efficacy in selectively sorting the two cell types, utilizing an interplay of magnetic (F_m) and hydrodynamic (F_d) forces. The resultant lateral magnetic force (F_l) precisely guided labeled cells to their respective collection points, underscoring the platform's accuracy and reliability in targeted cell sorting applications.

This methodology is vividly illustrated in the fluorescent image, which depicts a clear demarcation between the cell types along specified paths. The image evidences the precise segregation of the HeLa and A549 cells, with each cell type following a distinct trajectory toward its designated outlet. This sharp separation, based on the underlying principle of the microfluidic design, suggests a high level of efficiency in cell sorting. To validate the cell separation efficiency in this work, the percentage of A549 cells collected at the outlet can be used as a key metric. This percentage is calculated using the following formula:

$$A549\ Recovery\ Ratio\ at\ Outlet\ X\ (\%) = \frac{Number\ of\ A549\ cells\ at\ Outlet\ X}{Total\ number\ of\ cells\ at\ Outlet\ X} \times 100 \quad (1)$$

By applying this calculation, the ratio of collected A549 cells to the total number of cells (A549 and HeLa) present at the specific outlet is determined. This percentage reflects the effectiveness of the microfluidic device in selectively isolating A549 cells from the mixed population. A high percentage indicates successful separation, confirming that the system is capable of enriching the target A549 cells while minimizing the presence of HeLa cells at the outlet. This metric is crucial for assessing the performance and reliability of the separation process in real-world diagnostic or therapeutic applications.

While no prominent non-specific trapping of A549 cells on the ferromagnetic strips was observed during the experiments, occasional retention near the wire edge regions appeared in some fluorescence images. This suggests that a limited degree of cell accumulation may have occurred, potentially due to localized high-gradient magnetic fields or transient bead–cell interactions, as previously reported in similar magnetophoretic microfluidic systems [23, 24]. To minimize this risk, magnetic field intensity and flow rate were carefully optimized to maintain separation performance without inducing irreversible adhesion. Future designs may incorporate surface passivation strategies to further mitigate such effects [25]. The magnetic force applied in this system is governed by the configuration of the embedded permalloy strips ($Ni_{80}Fe_{20}$) integrated onto gold electrodes and subjected to an externally applied uniform magnetic field. This design closely parallels those reported in prior microfluidic magnetophoresis platforms. In such systems, lateral magnetic forces acting on magnetically labeled cells are typically estimated to fall within the range of 1 to 100 piconewtons (pN), a range that has been demonstrated to enable efficient lateral displacement while preserving cell viability and structural integrity. Recent studies further confirm that magnetic manipulation within this force range maintains cellular functionality, supporting its suitability for downstream biomedical applications.

Fig. 7 demonstrates a clear upward trend in the efficiency of A549 cell separation at different time points at outlet 2. The experiments were conducted separately at different time intervals: 2 minutes, 5 minutes, and 10 minutes. At 2 minutes, the percentage of A549 cells recovered is approximately 35.8% ± 2.3%, indicating moderate separation performance. By 5 minutes, this value increases to 58.2% ± 3.1%, and it reaches a peak of 84.4% ± 3.4% at the 10-minute mark. This progressive improvement suggests that the system becomes more effective over time in selectively isolating magnetically labeled A549 cells from the cell mixture. One possible explanation for this trend is the gradual stabilization of

conditions within the microfluidic channel. In the early minutes of operation, minor flow disturbances, initial transient effects, or uneven cell distribution at the inlet may have reduced separation efficiency. As time progresses, the system may reach a more equilibrated operating state in which labeled cells are more consistently deflected by the magnetic field. Additionally, any residual cells retained or delayed within the channel structure may gradually enter the outlet, contributing to the observed increase. This improvement over time reflects the importance of initial equilibration and system stabilization for achieving optimal separation. Once the internal conditions become consistent, the interaction between magnetic and hydrodynamic forces appears to be more uniform, enhancing the precision and reproducibility of cell sorting.

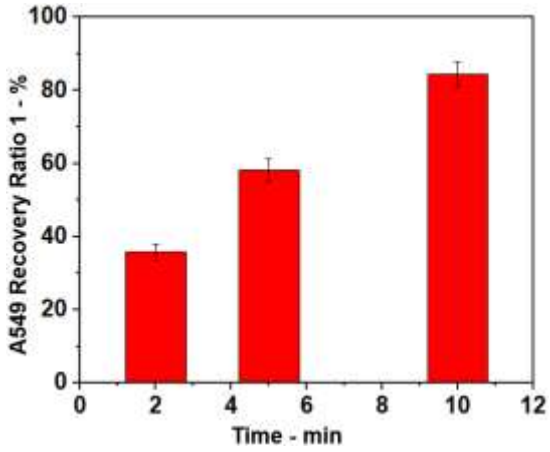

Figure 7. The recovery ratio of A549 cells at outlet 2 over time.

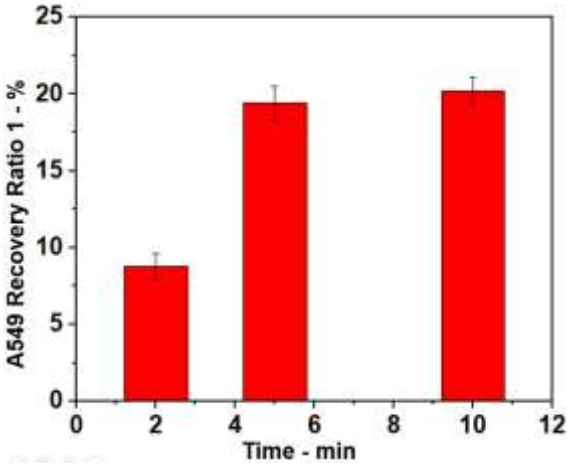

Figure 8. The recovery ratio of A549 cells at outlet 1 over time.

Fig. 8 illustrates the percentage of A549 cells recovered at output 1 over varying time intervals, revealing a similar overall trend in separation efficiency compared to output 2, but with notable quantitative differences. Specifically, output 1 consistently demonstrates lower recovery ratio, as anticipated, due to its collection of less effectively separated cells. Initially, at the 2-minute interval, the recovery ratio at output 1 is approximately 8.8% ± 1.1%, distinctly lower than that observed at output 2. This pattern persists across subsequent measurements; notably, at the 5-minute mark, the recovery ratio at output 1 is slightly above 19.4% ±1.4%, significantly less than the approximately 60% recorded at output 2. Even at the 10-minute interval, the highest time point measured, output 1 shows a recovery ratio of about 20.2% ± 1.8%, which contrasts markedly with the nearly 85% efficiency achieved at output 2. These findings underscore the differing efficiency between the two collection outlets, aligning with the expected performance characteristics of the microfluidic separation system. The increase in A549 recovery ratio over time at both outlets may partly result from non-specific adhesion of HeLa cells within the microfluidic channel, as partially illustrated in Figure 6. This reduces the number of HeLa cells reaching the outlets, thereby increasing the relative proportion of A549 cells detected.

This complementary result aligns with the assumption that output 1 collects the remaining cells that were not magnetically separated in output 2. The data at both outputs suggests that the system effectively channels most A549 cells to output 2, with output 1 collecting the residual, non-target cells (or those less magnetically responsive). The presence of A549 cells in output 1, although reduced, indicates some degree of overlap in the separation efficiency, possibly due to incomplete magnetic labeling or variations in the magnetic field strength. Further optimization might focus on reducing the cell population in output

1, perhaps by improving the magnetic responsiveness of the A549 cells or enhancing flow dynamics within the separation system.

Overall, the results from outputs 1 and 2 reveal a notable trend in which separation efficiency stabilizes progressively, particularly evident by the 10-minute interval. This stabilization is primarily attributed to the attainment of uniform flow dynamics, but may also involve secondary effects such as the delayed release of cells initially retained in the channel and the progressive reduction of non-specific HeLa cell retention near the ferromagnetic strip regions. As the flow stabilizes, the distribution of magnetic forces acting on the particles becomes uniform, enhancing the precision and reliability of the separation process. Simultaneously, the system clears transiently trapped or slowly responding cells, contributing to the increased and more consistent detection of A549 cells at the outlets. This phenomenon is particularly significant in microfluidic systems, where minor variations in flow conditions can substantially impact cell sorting accuracy. The observed reduction in variability at later stages of the experiment supports the conclusion that achieving stable flow conditions, along with minimizing unintended cell-surface interactions, is critical for optimal system performance. The equilibrium of flow velocity at approximately 10 minutes corresponds with steady separation efficiency at both outputs, indicating that the system operates effectively in sorting A549 and HeLa cells at this point. These findings emphasize the importance of meticulously controlled flow dynamics and surface passivation strategies to enhance the efficiency of magnetic-based cell separation techniques.

4. Conclusion

The microfluidic platform demonstrated in this work successfully employed lateral magnetophoresis to separate A549 lung cancer cells from HeLa cervical cancer cells with high efficiency. By incorporating ferromagnetic strips into the microchannel, the system was able to apply lateral magnetic forces that guided magnetically labeled A549 cells toward a designated outlet, achieving a maximum separation efficiency of 84.4%. Importantly, this efficiency was observed to increase progressively over the first 10 minutes of operation. Rather than indicating a change in flow rate, this trend likely reflects the stabilization of internal flow conditions, the gradual release of delayed or initially retained cells, and the more uniform deflection behavior of magnetically labeled cells as the system reached equilibrium. The results underscore the importance of initial equilibration time for optimized performance in magnetophoretic cell separation systems. With its ability to maintain consistent sorting outcomes and preserve cell viability, this platform holds strong promise for use in cancer diagnostics, circulating tumor cell isolation, and other biomedical applications requiring high-purity cell selection.

Acknowledgments

This work was funded by the Vietnam Ministry of Science and Technology under Grant ĐTĐL.CN-40/23. Van-Anh Bui was funded by the Master, Ph.D. Scholarship Programme of Vingroup Innovation Foundation (VINIF), code VINIF.2024.ThS.66.

References

[1] R. L. Siegel, K. D. Miller, A. Jemal, Cancer statistics, 2020, CA: A Cancer Journal for Clinicians, Vol. 70, No. 1, 2020, pp. 7-30, https://doi.org/10.3322/caac.21590.

[2] C. A. Panabières, K. Pantel, Challenges in Circulating Tumour Cell Research, Nature Reviews Cancer, Vol. 14, No. 9, 2014, pp. 623-631, https://doi.org/10.1038/nrc3820.
[3] C. Li, H. Wang, Y. Jiang, W. Fu, X. Liu, R. Zhong, B. Cheng, F. Zhu, Y. Xiang, J. He, W. Liang, Advances in Lung Cancer Screening and Early Detection, Cancer Biol. Med., Vol. 19, No. 5, 2022, pp. 591-608, https://doi.org/10.20892/j.issn.2095-3941.2021.0690.
[4] X. Fan, I. M. White, Optofluidic Microsystems for Chemical and Biological Analysis, Nature Photonics, Vol. 5, No. 10, 2011, pp. 591-597, https://doi.org/10.1038/nphoton.2011.206.
[5] G. Vona et al., Isolation by Size of Epithelial Tumor Cells, The American Journal of Pathology, Vol. 156, No. 1, 2000, pp. 57-63, https://doi.org/10.1016/S0002-9440(10)64706-2.
[6] B. Mostert, S. Sleijfer, J. A. Foekens, J. W. Gratama, Circulating Tumor Cells (CTCs): Detection Methods and their Clinical Relevance in Breast Cancer, Cancer Treatment Reviews, Vol. 35, No. 5, 2009, pp. 463-474, https://doi.org/10.1016/j.ctrv.2009.03.004.
[7] R. Pethig, Dielectrophoresis: Status of the Theory, Technology, and Applications, Biomicrofluidics, Vol. 4, No. 2, 2010, https://doi.org/10.1063/1.3456626.
[8] S. Riethdorf, H. Fritsche, V. Müller, T. Rau, C. Schindlbeck, B. Rack, W. Janni, C. Coith, K. Beck, F. Jänicke, S. Jackson, T. Gornet, M. Cristofanilli, K. Pantel, Detection of Circulating Tumor Cells In Peripheral Blood of Patients with Metastatic Breast Cancer: A Validation Study of the Cellsearch System, Clinical Cancer Research, Vol. 13, No. 3, 2007, pp. 920-928, https://doi.org/10.1158/1078-0432.CCR-06-1695.
[9] S. Miltenyi, W. Müller, W. Weichel, A. Radbruch, High Gradient Magnetic Cell Separation with MACS, Cytometry, Vol. 11, No. 2, 1990, pp. 231-238, https://doi.org/10.1002/cyto.990110203.
[10] D. Lin, L. Shen, M. Luo, K. Zhang, J. Li, Q. Yang, F. Zhu, D. Zhou, S. Zheng, Y. Chen, J. Zhou, Circulating Tumor Cells: Biology and Clinical Significance, Signal Transduction and Targeted Therapy, Vol. 6, No. 1, 2021, Article number: 404, https://doi.org/10.1038/s41392-021-00817-8.
[11] D. R. Gossett, W. M. Weaver, A. J. Mach, S. C. Hur, H. T. K. Tse, W. Lee, H. Amini, D. D. Carlo, Label-free Cell Separation and Sorting in Microfluidic Systems, Analytical and Bioanalytical Chemistry, Vol. 397, No. 8, 2010, pp. 3249-3267, https://doi.org/10.1007/s00216-010-3721-9.
[12] M. Xu, H. Zhao, J. Chen, W. Liu, E. Li, Q. Wang, L. Zhang, An Integrated Microfluidic Chip and Its Clinical Application for Circulating Tumor Cell Isolation and Single-Cell Analysis, Cytometry Part A, Vol. 97, No. 1, 2020, pp. 46-53, https://doi.org/10.1002/cyto.a.23902.
[13] K. A. Hyun, K. Kwon, H. Han, S. I. Kim, H. I. Jung, Microfluidic Flow Fractionation Device for Label-Free Isolation of Circulating Tumor Cells (CTCs) from Breast Cancer Patients, Biosensors and Bioelectronics, Vol. 40, No. 1, 2013, pp. 206-212, https://doi.org/10.1016/j.bios.2012.07.021.
[14] M. M. Ferreira, V. C. Ramani, S. S. Jeffrey, Circulating Tumor Cell Technologies, Molecular Oncology, Vol. 10, No. 3, 2016, pp. 374-394, https://doi.org/10.1016/j.molonc.2016.01.007.
[15] K.I. Cima, C. W. Yee, F. S. Iliescu, W. M. Phyo, K. H. Lim, C. Iliescu, M. H. Tan, Label-free Isolation of Circulating Tumor Cells in Microfluidic Devices: Current Research and Perspectives, Biomicrofluidics, Vol. 7, No. 1, 2013, Article ID: 011810, https://doi.org/10.1063/1.4780062.
[16] N. Lu, H. M. Tay, C. Petchakup, L. He, L. Gong, K. K. Maw, S. Y. Leong, W. W. Lok, H. B. Ong, R. Guo, K. H. H. Li, H. W. Hou, Label-free microfluidic cell sorting and detection for rapid blood analysis, Lab on a Chip, Vol. 23, 2023, pp. 1226–1257, https://doi.org/10.1039/D2LC00904H.
[17] M. Cristofanilli, G. T. Budd, M. J. Ellis, A. Stopeck, J. Matera, M. C. Miller, J. M. Reuben, G. V. Doyle, W. J. Allard, L. W. M. M. Terstappen, D. F. Hayes, Circulating Tumor Cells, Disease Progression, and Survival in Metastatic Breast Cancer, New England Journal of Medicine, Vol. 351, No. 8, 2004, pp. 781-791, https://doi.org/10.1056/NEJMoa040766.
[18] L. Luo, Y. He, Magnetically Driven Microfluidics for Isolation of Circulating Tumor Cells, Cancer Medicine, Vol. 9, No. 12, 2020, pp. 4207, https://doi.org/10.1002/cam4.3077.
[19] J. Lee, O. Sul, S. B. Lee, Enrichment of Circulating Tumor Cells from Whole Blood Using a Microfluidic Device for Sequential Physical and Magnetophoretic Separations, Micromachines, Vol. 11, No. 5, 2020, pp. 481, https://doi.org/10.3390/mi11050481.
[20] Z. Qiao, X. Teng, A. Liu, W. Yang, Novel Isolating Approaches to Circulating Tumor Cell Enrichment Based on Microfluidics: A Review, Micromachines, Vol. 15, No. 6, 2024, pp. 706, https://doi.org/10.3390/mi15060706.

[21] N. Pamme, Magnetism and Microfluidics, Lab on a Chip, Vol. 6, No. 1, 2006, pp. 24-38, https://doi.org/10.1039/b513005k.
[22] C. W. Shields IV, C. D. Reyes, G. P. López, Microfluidic Cell Sorting: A review of the Advances In The Separation Of Cells From Debulking To Rare Cell Isolation, Lab on a Chip, Vol. 15, No. 5, 2015, pp. 1230-1249, https://doi.org/10.1039/c4lc01246a.
[23] J. H. Kang, S. Krause, H. Tobin, A. Mammoto, M. Kanapathipillai, D. E. Ingber, A Combined Micromagnetic-Microfluidic Device for Rapid Capture and Culture of Rare Circulating Tumor Cells, Lab on a Chip, Vol. 12, No. 12, 2012, pp. 2175, https://doi.org/10.1039/c2lc40072c.
[24] M. Xavier, R. O. C. Oreffo, H. Morgan, Skeletal Stem Cell Isolation: A Review on the State-of-the-art Microfluidic Label-free Sorting Techniques, Biotechnology Advances, Vol. 34, No. 5, 2016, pp. 908-923, https://doi.org/10.1016/j.biotechadv.2016.05.008.
[25] M. Strozyk, Gold Nanoparticles in Polymeric Matrices for Biomedical Applications, 2017.